JBC RESEARCH ARTICLE

Structural analysis of P450 AmphL from *Streptomyces nodosus* provides insights into substrate selectivity of polyene macrolide antibiotic biosynthetic P450s

Received for publication, August 30, 2021, and in revised form, February 14, 2022 Published, Papers in Press, February 18, 2022,
https://doi.org/10.1016/j.jbc.2022.101746

Jose A. Amaya[1], David C. Lamb[2], Steven L. Kelly[2], Patrick Caffrey[3], Vidhi C. Murarka[1], and Thomas L. Poulos[1,*]

From the [1]Departments of Molecular Biology and Biochemistry, Pharmaceutical Sciences, and Chemistry, University of California, Irvine, California, USA; [2]Faculty of Health, Medicine and Life Sciences, Swansea University, Swansea, UK; [3]School of Biomolecular and Biomedical Science, University College Dublin, Belfield, Dublin 4, Ireland

Edited by F. Peter Guengerich

AmphL is a cytochrome P450 enzyme that catalyzes the C8 oxidation of 8-deoxyamphotericin B to the polyene macrolide antibiotic, amphotericin B. To understand this substrate selectivity, we solved the crystal structure of AmphL to a resolution of 2.0 Å in complex with amphotericin B and performed molecular dynamics (MD) simulations. A detailed comparison with the closely related P450, PimD, which catalyzes the epoxidation of 4,5-desepoxypimaricin to the macrolide antibiotic, pimaricin, reveals key catalytic structural features responsible for stereo- and regio-selective oxidation. Both P450s have a similar access channel that runs parallel to the active site I helix over the surface of the heme. Molecular dynamics simulations of substrate binding reveal PimD can "pull" substrates further into the P450 access channel owing to additional electrostatic interactions between the protein and the carboxyl group attached to the hemiketal ring of 4,5-desepoxypimaricin. This substrate interaction is absent in AmphL although the additional substrate -OH groups in 8-deoxyamphotericin B help to correctly position the substrate for C8 oxidation. Simulations of the oxy-complex indicates that these -OH groups may also participate in a proton relay network required for O_2 activation as has been suggested for two other macrolide P450s, PimD and P450eryF. These findings provide experimentally testable models that can potentially contribute to a new generation of novel macrolide antibiotics with enhanced antifungal and/or antiprotozoal efficacy.

Streptomyces nodosus produces the important antifungal and antiprotozoal polyene macrolide antibiotic amphotericin B (Fig. 1) (1). The ability of amphotericin B to act as an antifungal/antiprotozoal agent centers on its ability to interact with sterols, especially ergosterol, an essential component in fungal and protozoa cell membranes. Nevertheless, clinically amphotericin B has a number of undesirable side effects, particularly nephrotoxicity, owing to its ability to bind a variety of other sterols (2, 3). As a result, there is considerable interest in developing amphotericin analogs that are more selective and efficacious.

The macrolactone core of amphotericin B is the product of a large polyketide synthase. Three late stage amphotericin B biosynthetic steps occur in the following order: the AmphN cytochrome P450 functions in conversion of the C41 methyl branch to a carboxyl group, a mycosamine sugar is added at C19, and the AmphL cytochrome P450 hydroxylates C8. The final AmphL-catalyzed step is shown in Figure 1. Herein, we describe the 2.0 Å crystal structure of AmphL in complex with the final product, amphotericin B. Utilizing molecular dynamics (MD) simulations, we compare AmphL with the closely related cytochrome P450, PimD, to gain a better understanding of the structural basis for macrolide antibiotic substrate specificity in these two closely related P450s.

Results and discussion

AmphL characterization

The spectra of oxidized AmphL and the reduced CO spectrum without and with substrate are shown in Figs. S1 and S2. The reduced CO spectrum gives approximately a 50:50 mix of P420 and P450. This is not too uncommon for substrate-free P450 (4, 5). The substrate itself, a mixture of 8-deoxyamphotericin A and B, exhibits substantial absorbance in the 400 nm range which precludes estimating the amount of P420 and P450 in the substrate-bound complex (Fig. S2). Similarly, the substrate interferes with the usual low-to-high spin shift used to estimate spectral dissociation constants (K_D, Fig. S3). The change in optical density at 395 nM increases with increasing at saturates near 2 μM substrate indicating that the K_D is in the low μM range (Fig. S3). We were unsuccessful in demonstrating product formation using non-native redox partners, spinach ferredoxin and spinach ferredoxin reductase, or H_2O_2.

AmphL overall structure analysis

We were not successful in crystallizing AmphL with its substrate bound, but we were able to solve and refine the 2.0 Å structure of AmphL complexed with the final product, amphotericin B (Table 1).

* For correspondence: Thomas L. Poulos, poulos@uci.edu.

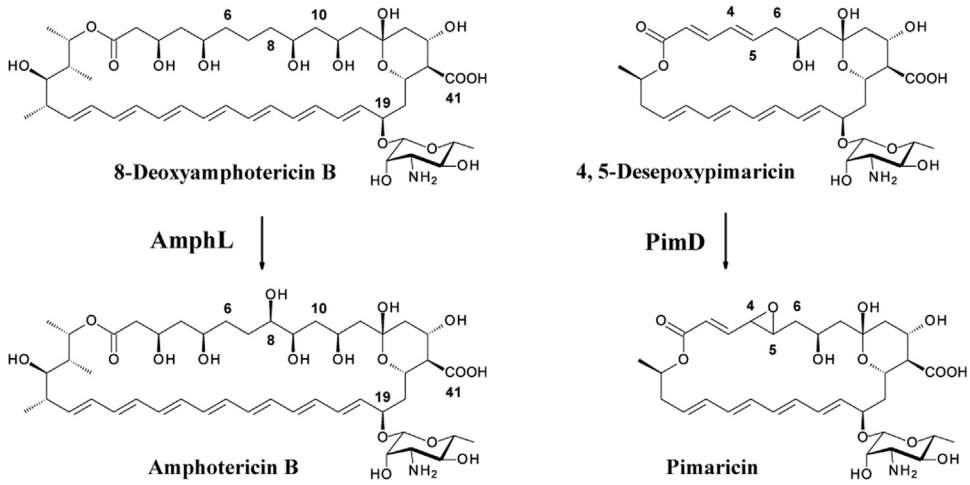

Figure 1. Structures of relevant polyene macrolide antibiotics. AmphL oxidizes 8-deoxyamphotericin B at the C8 position. PimD catalyzes the epoxidation of 4,5-desepoxypimaricin across the C4-C5 double bond.

AmphL crystallizes in space group $P2_12_12_1$ with a dimer in the asymmetric unit. The rms difference in Cα atoms between the two molecules is 0.2 Å and 0.14 Å for the amphotericin B bound to AmphL, indicating no significant difference between the two molecules. AmphL exhibits the traditional P450 fold (Fig. 2). The most highly conserved regions are the long I helix that runs over the distal surface of the heme and the L helix on the proximal side that provides the Cys thiolate heme iron ligand. Catalytically, AmphL adds an -OH group to C8 of 8-deoxyamphotericin B and as shown in Figure 2, the C8 -OH group is located 3.3 Å from the heme iron which is consistent with C8 being correctly positioned for stereo- and regioselective hydroxylation. Therefore, the product complex is a true representation of how substrate will bind in the AmphL active site.

Table 1
Data collection and refinement statistics

PDB code	7SHI
Space group	P 2_1 2_1 2_1
Unit cell (Å and degrees)	73.458 68.154 147.529 90 90 90
Resolution range (Å)	33.88–2.0
Highest resolution shell	2.07–2.00
Total reflections	101,378 (9935)
Unique reflections	50,714 (3950)
Multiplicity	2.0 (2.0)
Completeness (%)	94.94 (79.15)
Mean I/sigma(I)	11.28 (3.42)
Wilson B-factor	23
R-merge	0.0945 (1.907)
R-meas	0.1336 (2.696)
R-pim	0.0945 (1.907)
CC1/2	0.949 (0.336)
CC*	0.987 (0.709)
Reflections used in refinement	48,258 (3949)
Reflections used for R-free	1999 (157)
R-work	0.1918 (0.2235)
R-free	0.2492 (0.3072)
CC(work)	0.965 (0.852)
CC(free)	0.947 (0.744)
Number of nonhydrogen atoms	6648
Macromolecules	6169
Ligands	101
Solvent	378
Protein residues	786
RMS(bonds)	0.007
RMS(angles)	0.96
Ramachandran favored (%)	97.43
Ramachandran allowed (%)	1.93
Ramachandran outliers (%)	0.64
Rotamer outliers (%)	5.75
Clashscore	12.94
Average B-factor	27.86
Macromolecules	27.81
Ligands	16.75
Solvent	31.67

Numbers in () are for the highest resolution shell. Statistics were generated by the "Table 1" utility in Phenix.

AmphL substrate access channel

In describing substrate binding, it is instructive to compare the structure of AmphL with PimD (6), a P450 that catalyzes the 4,5 epoxidation of 4,5-desepoxypimaricin to give pimaricin (Fig. 1). Pimaricin is a smaller molecule than amphotericin B, being a 26-member ring *versus* 38, which amounts to approximately 7 Å difference in length along the long axis. These two P450s share 55% sequence identity at the amino acid level and the rms difference in Cα positions is 0.9 Å for 340 residues. Consequently, both P450s are structurally very similar. Unlike a majority of P450s where substrate entry occurs near the F/G loop connecting the F and G helices, these two macrolide-binding P450s may use another channel as illustrated in Figure 2. This channel runs parallel to the P450 I helix over the surface of the heme and provides a wide opening for the elongated axis of the substrate to slip into the active site. In many other P450s, the F/G helical region undergoes substantial conformational changes between the substrate-free and -bound states thus providing the opening required for substrate entry (7). In PimD, however, a comparison of the substrate-free and -bound structures (6) shows a less dramatic change in the F/G helical region. If substrate entry occurred *via* the traditional F/G helical route, then the substrate would need to enter, presumably, with the long axis oriented downward toward the heme so that it can fit through the opening. This would need to be followed by a 90° rotation as it enters the active site in order to correctly position the C4-C5 double bond for epoxidation, and this would require extremely large conformational changes. On the other hand, access *via*

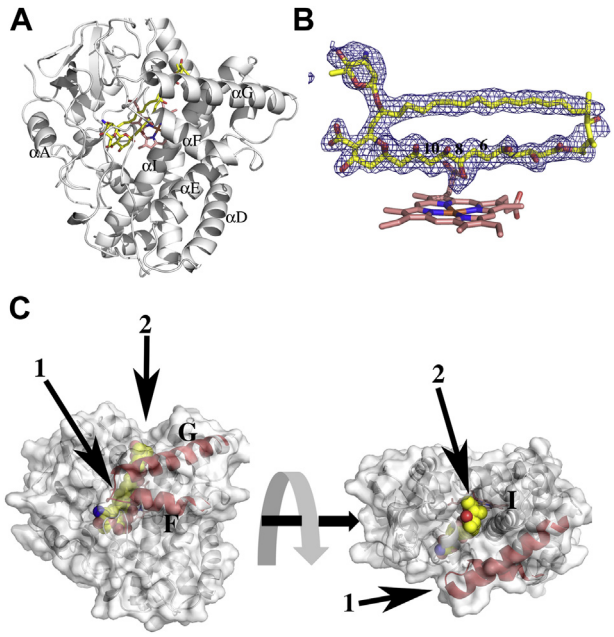

Figure 2. Overall structure of AmphL. *A*, AmphL exhibits the traditional P450 fold. The I helix runs over the surface of the heme and provides the conserved Thr/Ser and Asp generally thought to be part of a proton relay network required for O_2 activation. *B*, a polder difference electron density map with the amphotericin B omitted from the calculation contoured at 3.0σ. This is the product of the AmphL reaction so the C8 carbon has the -OH group attached. *C*, surface depiction of AmphL illustrating the two possible substrate entry channels. Channel 1 is situated near the loop connecting the F and G helices and is generally thought to be the main access route to the active site in many P450s. In several P450s, this region undergoes a large open/close switch between the substrate-free (open) and substrate-bound (closed) conformers. PimD and AmphL have a second access channel, channel 2, roughly perpendicular to channel 1 that runs parallel to the I helix. This provides ready entry of the long axis of substrates without requiring substantial conformational adjustments that are likely required if channel 1 is the main entry route.

channel 2 (Fig. 2) requires little conformational gymnastics since the long axis of the substrate can enter without the strict requirement for any major reorientation while more fine-tuned interactions control the correct positioning for P450 substrate epoxidation.

AmphL and PimD substrate–protein interactions

As shown in Figure 3, with one main exception, many of the amino acid residues interacting with the long substrate macrolactone ring in PimD and AmphL are conserved (Fig. 3). The exception is Phe81 in PimD which is Leu83 in AmphL. The larger Phe81 would sterically clash with a larger substrate and thus may limit the size of the substrate that can bind stably in the P450 active site. At the "back wall" of the binding cavity, both the six-member hemiketal and mycosamine rings are similarly positioned in PimD and AmphL. This back wall of the substrate-binding pocket where the two rings bind defines how deep the substrate can penetrate into the binding pocket which, in turn, anchors the site of hydroxylation to be precisely and correctly positioned over the heme iron. As might be expected with a larger substrate, AmphL has a more open active site (Fig. 4).

The accessible surface area of the enzyme active site cavity is 867 $Å^2$ in AmphL compared to 545 $Å^2$ in PimD. The most notable difference is near the entry to channel 2 formed in part by a loop that connects the H and I helices. Interactions between this loop and neighboring groups hold the entry to channel 2 more open in AmphL. In direct contrast, PimD lacks these interactions. This additional stabilization in AmphL is accomplished by some key amino acid differences. First, AmphL has Pro217 where PimD has Leu219. Second, in AmphL, Arg201 H-bonds with both Glu219 and the peptide carbonyl O atom of Pro217, which anchors the connecting loop between the P450 H and I helices in place. PimD is missing these H-bonding possibilities and as a result, the H/I connecting segment is free to move resulting in a tighter entry to the substrate-binding channel. Indeed, the H/I connecting segment moves about 3 Å in P450 PimD when its substrate binds (6).

AmphL and PimD catalytic residues

AmphL and PimD retain key active site residues generally considered to be important for P450 O_2 activation. A majority of P450s have a Thr residue (Thr252 in P450cam) adjacent to where O_2 will coordinate the heme iron (7). Together with Asp251 (P450cam), these two residues participate in a proton relay network required for O_2 activation (8). AmphL has a functionally equivalent Ser236 (Ser238 in PimD) rather than Thr. A Thr at this position would cause too much steric crowding with the nearby substrate. AmphL retains the catalytically important Asp, Asp235 (Asp237 in PimD). Weak electron density associated with the Asp235 carboxyl group indicates that Asp235 is free to undergo the rotameric changes required for delivery of protons to the enzyme active site. This is unlike P450cam where Asp251 is anchored in place by ion pairs with Lys178 and Arg186. With P450cam, the binding of its Fe_2S_2 ferredoxin redox partner results in a rupture of the Asp251 ion pairs thereby releasing Asp251 to serve its role in proton-coupled electron transfer (4). AmphL appears not to require a similar effector role of redox partner binding. Despite these conserved residues thought to be important for O_2 activation, Kells *et al.* (6) argue that the PimD epoxidation reaction more likely proceeds using H_2O_2 as the oxidant, thereby bypassing the requirement for electron transfer and O_2 activation. This hypothesis was based on the fact that H_2O_2 but not the oxo donors, iodosobenzene and peroxynitrite that form the traditional P450 Compound I Fe(IV)=O center, gives the correct catalytic product. Less convincing was the structural argument that water remains about 3.3 Å from the heme iron in the substrate complex and the I helix structure near the O_2 site lacks the water molecule that contributes to the local distortion of the I helix as observed in other P450s. However, the local I helix structure environment, including solvent, is very much the same in AmphL and PimD, yet AmphL utilizes the traditional P450 mechanism. It also is known that, at least in P450cam, the local I helix and solvent structure changes in the O_2 complex so it may not be appropriate to draw too many detailed mechanistic conclusions based on the AmphL resting state ferric structure. Nevertheless, PimD does carry out an epoxidation rather than

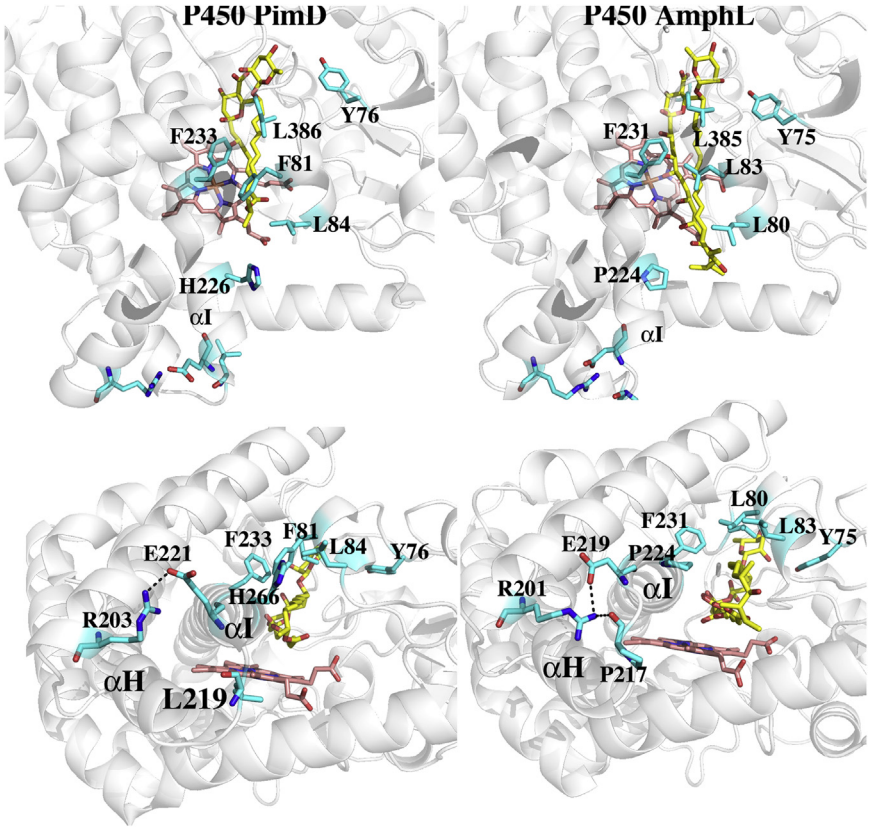

Figure 3. Comparison of the PimD and AmphL active sites. Several residues directly contacting the substrate are conserved. There are, however, key differences that may contribute to substrate specificity. P450 PimD has the larger Phe81 where AmphL has Leu83. The larger Phe81 in PimD could possibly limit the binding of much larger substrates. The binding of the larger amphotericin B would certainly result in steric clashes with Phe81 without some readjustments. In AmphL, the entry to the binding channel is more rigidly held in place by H-bonding interactions involving Glu219, Arg201, and Pro217 in AmphL. PimD has no similar rigidifying interactions suggesting that PimD would not be able to pack as tightly around a long macrolide like amphotericin B.

the traditional P450 hydroxylation so a different mechanism is certainly feasible.

Modeling the AmphL oxy complex

Ser236 in AmphL is close enough to substrate -OH groups for H-bonding interactions. In the oxy complex, there is the additional possibility that the O_2 molecule can not only interact with Ser236 but also with the substrate C9 and C11 -OH groups. To obtain some mechanistic insight into this possibility, we modeled the AmphL-oxy complex using the P450cam-oxy structure (9) as a template and carried out a 50 ns MD simulation. The center of mass of the C9 and C11 -OH groups and the distal O_2 oxygen atom is <4.0 Å 58% of the time. In addition, a water molecule is within 3.5 Å of the C9 -OH 85% of the time. A representative snapshot from the MD simulation is shown in Figure 5. There is a continuous water network channel from the protein surface to the O_2 molecule that involves the C9 and C11 substrate -OH groups and Ser236. This raises the possibility that the AmphL

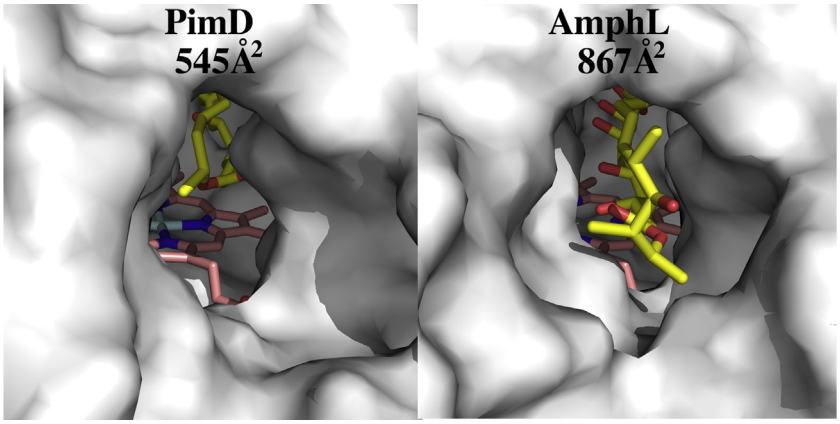

Figure 4. Comparison of the active site cavity in PimD and AmphL. AmphL has a more open pocket in order to accommodate the longer substrate.

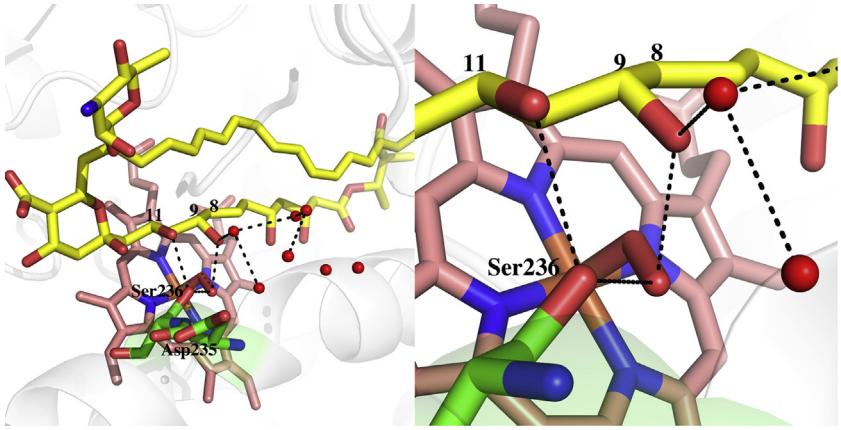

Figure 5. One snapshot from the MD simulation of the AmphL-oxy complex illustrating the possible water network connecting the surface where Asp235 is located to the iron-linked O_2 molecule. The *dashed line* indicates potential H-bonding interactions where the distance <3.0 Å.

substrate itself can participate in O_2 activation by donating a proton to the distal O_2 oxygen atom. Such a mechanism was first suggested for another macrolide P450, P450eryF (10). P450eryF has an Ala rather than Ser or Thr at this position, and analysis of substrate analogs showed that a substrate -OH group near the O_2 molecule is essential for P450eryF catalysis (10). Substrate-assisted catalysis has also been suggested for PimD (6). While such substrate assistance in O_2 activation may or may not be a general feature of macrolide biosynthetic P450s, the macrolide substrate itself provides ample possibilities.

Molecular dynamics and substrate specificity

Given that AmphL and PimD are structurally so similar, it is not unexpected that simple molecular modeling reveals that the AmphL substrate can fit into the P450 PimD active site and vice-versa. However, catalytically, it has previously been shown that AmphL does not hydroxylate or epoxidize the PimD substrate *in vivo* or *in vitro* (11). To obtain further insight into substrate specificity and catalysis, we carried out four different MD simulations of the enzyme-substrate complexes: AmphL and PimD in complex with 8-deoxyamphotericin B and AmphL and PimD in complex with 4,5-desepoxypimaricin. To generate the structure of AmphL in complex with the PimD substrate and vice-versa, we simply superimposed the crystal structures and used the coordinates of the substrate. In each case, five 100 ns MD simulations were run with each run starting with the same equilibrated structure but with different starting velocities. A simple way to follow stability of the bound substrate is to calculate what fraction of time during the MD runs the site known to be oxidized stays close to the heme iron. These results are presented in Table 2.

In the AmphL-8-deoxyamphotericin B complex, the C8 atom, which is the site of oxidation, remains close to the heme iron in 49.3% of the frames while the neighboring sites are much lower (Table 2). Whereas in PimD-8-deoxyamphotericin B complex, the C8 atom remains close to the heme iron a lower 39.7% of the frames while C10 is never <5.5 Å from the heme iron. The reason for this difference is that the substrate penetrates deeper in the active site which places, on average, the C8 and C10 carbons farther from the heme iron than in AmphL. In the PimD-4,5-desepoxypimaricin complex, the epoxide product is formed across the C4-C5 double bond and as shown in Table 2, C4 and C5 remain close to the heme iron while in the AmphL-4,5-desepoxypimaricin complex, only C6 remains close to the heme iron thus explaining the lack of activity of AmphL toward 4,5-desepoxypimaricin (11). This is consistent with the differences seen in the 8-deoxyamphotericin B complexes: both macrolide substrates are able to penetrate slightly further into the active site in PimD. A possible reason for this difference involves the interactions between the hemiketal and mycosamine rings and the back wall of the substrate-binding pocket. Figure 6 is the last frame taken from one of the five MD simulations and clearly shows that the hemiketal is positioned further into the active site in P450 PimD. We propose that this difference involves tighter interactions between the carboxyl group attached to the hemiketal ring and the surrounding protein structure in P450 PimD over that found in AmphL. In PimD, Arg279 remains close to the carboxyl group. In the five 100 ns MD simulations, the distance between the center of mass of the two carboxyl groups and the NE atom of Arg279 remains <3.5 Å 89% of the time and <3.0 Å 48% of the time, so this ion-pair/H-bonding interaction is quite stable. In sharp contrast, Arg279 is replaced by Lys277 in AmphL and in both the crystal structure and MD simulations, Lys277 points away from the substrate carboxyl group and in the MD simulations, Lys277-carboxyl distance is <3.5 Å only 12% of the time. This additional interaction in PimD thus helps to pull and hold the substrate further into the enzyme active site. What AmphL loses in missing this interaction, it gains in how some of its substrate -OH groups interact with the I helix. The C11 and C13 substrate -OH groups can H-bond with Ser236 (Fig. 6). The center of mass of the two substrate -OH groups in 8-deoxyamphotericin B remain <3.5 Å from Ser236 81.7% of the time and only 19.8% of the time in PimD.

To obtain further insight into the substrate-binding properties of AmphL and PimD, we turned to steered molecular dynamics (SMD). In a SMD simulation, a force is

Table 2
Various distances from the indicated substrate carbon atom to heme iron

Substrate carbon atom	AmphL-amp	PimD-amp	AmphL-pim	PimD-pim
C6-amp	17.7%	14.6%		
C8-amp	49.3%	39.7%		
C10-amp	12.9%	0%		
C4-pim			18.9%	89.6%
C5-pim			18.7%	58.1%
C6-pim			94.4%	69.4%

The percentages given are the % of a total of 25,000 frames from 5 to 100 ns MD simulations where the distance is <5.5 Å. amp = 8-deoxyamphotericin B and pim = 4,5-desepoxypimaricin.

applied to a protein ligand in order to pull or push the ligand out of the active site–binding pocket. This method is useful in exploring potential entry/exit routes for ligands (12), with the assumption that the path that requires the least pull/push energy is the most favorable. In our case, we already have a clear idea on the path of substrate entry into PimD and AmphL, so we used SMD to compare the work required to remove the same substrate from AmphL and PimD. This provides a measure of relative affinity in addition to energetic barriers to conformational changes required for substrate dissociation. The vector that defines the direction of push has the tail end of the vector at Cα of a residue at the back end of the substrate-binding pocket, and the vector head is a ligand atom near the entry of the active site (Fig. 7). In order to prevent the protein from moving rather than the substrate, the vector tail Cα and Cα of several surrounding residues were restrained during the SMD run. The SMD run was repeated 100 times using frames taken from the last 10 ns of a 20 ns production MD run. Over the course of each SMD run, the work required as a function of distance is saved every 2.8 ps. The mean work over all 100 frames is converted to the potential of mean force using the Jarzynski equality (13):

$$\exp(-\Delta G / k_B T) = \exp\langle(-W / k_B T)\rangle_A$$

More work is required to push the substrate from the AmphL active site compared to that required for PimD (Fig. 7). This reflects what we observe in the crystal structure: AmphL packs more tightly around the tail end of 8-deoxyamphotericin B near the substrate entry pocket than PimD owing, at least in part, to additional H-bonding interactions at the entry of the access channel. Consequently, this helps to stabilize P450-substrate interactions. We also carried out similar SMD runs for 4,5-desepoxypimaricin escaping the AmphL and PimD active sites (Fig. 7). Here, there is very little difference indicating that the P450-substrate interactions and conformational changes required when the smaller substrate dissociates is approximately the same for both enzymes.

Our results suggest that AmphL and PimD may be able to bind each other's substrate although the SMD results indicate that AmphL binds more tightly to its own substrate 8-deoxyamphotericin B than does PimD. While the MD work indicates that AmphL may be able to bind the PimD substrate, the inability for AmphL to pull substrates further into the active site could contribute to why AmphL is unable to oxidize 4,5-desepoxypimaricin (11). In sharp contrast, the closely related P450 NysL (a P450 which is involved in the late-stage oxidative tailoring of the macrolide antibiotic nystatin (14)) is able to oxidize 4,5-desepoxypimaricin at C6 (11). The NysL substrate, 10-desoxynystatin, has the same size macrolide ring structure as the AmhpL substrate, yet NysL oxidizes C10 rather than C8. If we assume that the site to be oxidized must be similarly positioned over the heme iron, then in NysL, its substrate does not penetrate as far into the active site as seen in the AmphL situation. If true, then 4,5-desepoxypimaricin would also not penetrate in as far which would place C6 in a more optimal position for oxidation. Overall, the available structural results and known substrate oxidation profiles described herein support the overall view that the back wall of these macrolide P450s that interact with the two six member rings plays a major role in controlling how far a substrate penetrates into the active site thus enabling proper positioning of the substrate for regio- and stereo-selective oxidation.

Conclusions

Our comparison between the two closely related macrolide oxidizing P450s, AmphL and PimD, provides important new insights into the subtle structural differences that control

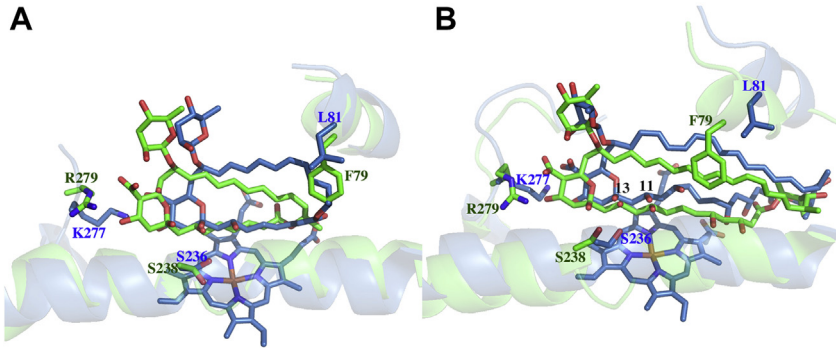

Figure 6. The last frame form one of the 5100 ns MD simulations. *A*, PimD (*green*) and AmphL (*blue*) in complex with 4,5-desepoxypimaricin. Arg279 in AmphL interacts with the substrate carboxyl which helps to pull the substrate further into the active site. This interaction is missing in AmphL since Lys277 points "down" and away from the carboxyl group in both the crystal structure and MD simulations. *B*, PimD (*green*) and AmphL (*blue*) in complex with 8-deoxyamphotericin B. As with 4,5-desepoxypimaricin, PimD pulls the substrate further into the active site. In AmphL, Ser236 is able to form H-bonding interactions with the C11 and C13 -OH groups while these interactions are missing in PimD.

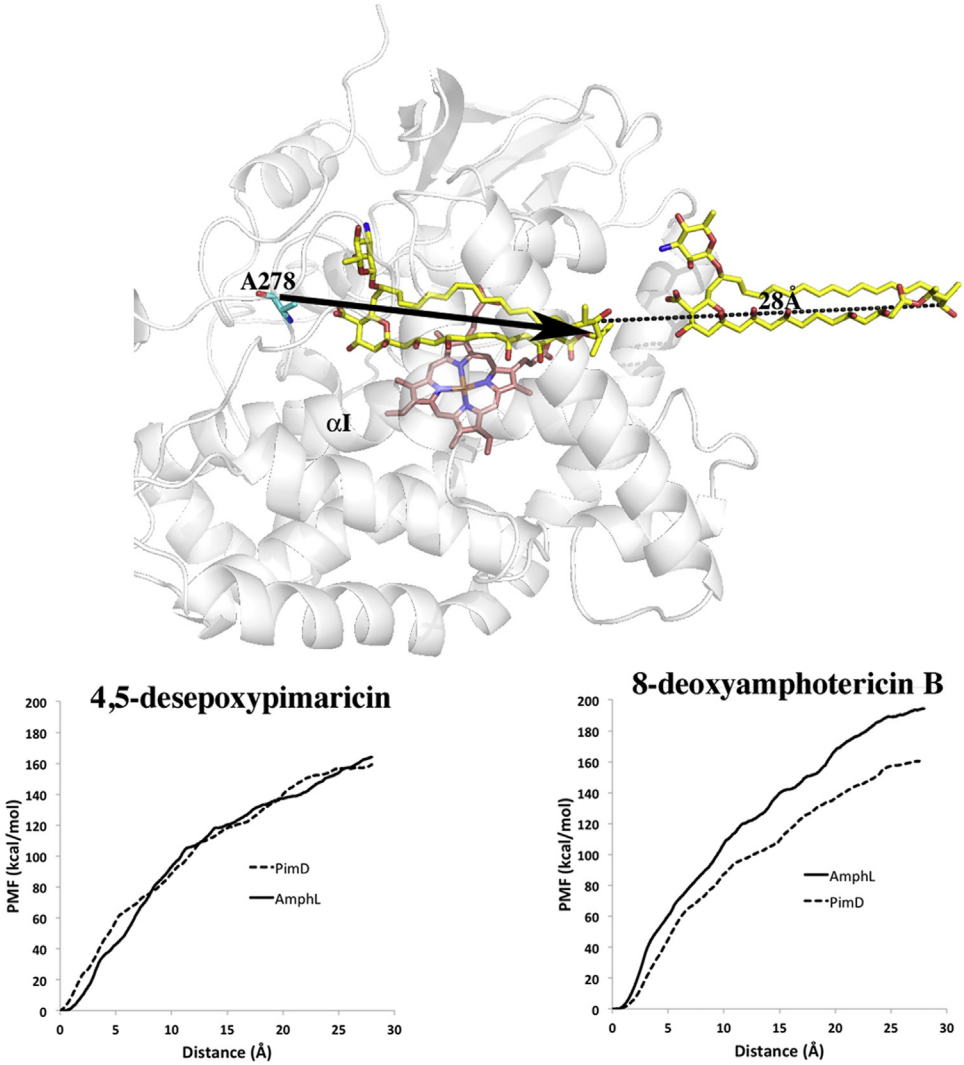

Figure 7. The protein model shows the starting and final position of 8-deoxyamphotericin B for a typical SMD run. The tail end of the forcing vector was placed at Cα of Ala278 and the head at C15 of the substrate. A force of 30 kcal mol^{-1} $Å^{-2}$ was applied over a period of 2.8 ns at 10 Å/ns giving a total distance of 28 Å. The two plots show the resulting PMF as a function of distance. A significantly greater force is required to dissociate the AmphL substrate from AmphL while the force required for extrusion of the PimD substrate is about the same in both P450s. PMF, potential of mean force; SMD, steered molecular dynamics.

regio- and stereo-selective hydroxylation of their respective substrates. Using the AmphL structure presented herein, modeling and MD simulations provide new insights into P450 macrolide substrate binding and oxidation (11). It is not uncommon in P450s for ligands to bind yet not be substrates which underscore the importance of the precise positioning of the substrate relative to the heme prior to oxidation. The MD simulations where P450 substrates were swapped indicate that protein-substrate interactions with the two six-member rings controls how far the substrate can penetrate into the long access channel. The ability of PimD to provide an additional electrostatic interaction with the hemiketal carboxyl group helps to pull its macrolide substrate further into the active site and thereby correctly position C4 and C5 for epoxidation. In contrast, AmphL lacks this mechanistic possibility but instead relies on interactions between its substrate -OH groups and parts of the P450 I helix to help position the substrate for C8 oxidation. Finally, it is potentially possible to use these structural insights as a guide to genetically engineer P450s with different oxidation profiles to generate novel macrolide antifungal and/or antiprotozoal antibiotics with enhanced efficacy and reduced toxic side effects.

Experimental procedures

AmphL cloning

The expression plasmid pQE80L-*amphL* produces a recombinant AmphL protein containing an N-terminal hexahistidine tag. To construct this plasmid, the *amphL* gene was amplified by PCR from *S. nodosus* genomic DNA using the following primers: AmphL-F (5′ ACGTGGATCCATGGTC AACCCGACACCGCCGCC 3′) and AmphL-R (5′ GATC AAGCTTACCAGGTGACGGGCAGTTCG 3′). The thermostable DNA polymerase was Deep Vent DNA Polymerase (New England BioLabs). Initial template denaturing was carried out at 95 °C for 4 min. The synthesis cycle consisted of

annealing at 62 °C for 1 min, extension at 72 °C for 2 min, and denaturation at 95 °C for 1 min. This was repeated 30 times. The reaction mixture was then incubated at 72 °C for 7 min and finally held at 4 °C. The amplified *amphL* gene was cloned between the *BamHI* and *HindIII* sites of the *Escherichia coli* expression plasmid pQE80L. Resequencing confirmed that the recombinant AmphL coding sequence was error-free.

AmphL protein expression and purification

Recombinant *S. nodosus* AmphL was expressed in *E. coli*. C41 (DE3) cells (Merch). A single-plated colony of transformed bacteria was used to inoculate 5 ml of LB media (10 g tryptone, 25g yeast extract, and 10g NaCl per liter) containing 100 μg/ml ampicillin. The overnight culture was incubated at 37 °C at 250 rpm and then diluted (1:100) into 1.5 l of Terrific Broth media (24 g yeast extract, 12 g tryptone, and 2 g peptone per liter) supplemented with 100 μg/ml ampicillin, 125 mg/ml thiamine, and 375 μl of trace elements salt solution. The cultures were grown at 37 °C until $A_{600} \sim 1.5$ was reached. δ-aminolevulinic acid (1 mM final concentration) was added to improve heme synthesis for the expression of heme-bound AmphL recombinant protein. Protein production was initiated following the addition of IPTG (1 mM final concentration), and the cell growth was continued for an additional 24 h at 20 °C and 190 rpm. Subsequently, the cells were harvested by centrifugation (1850*g* for 20 min) and the supernatant was discarded. The red cell pellet containing recombinant AmphL was freeze-thawed and resuspended in buffer A (50 mM K_2HPO_4 pH 7.5, containing 100 mM NaCl and 10 mM imidazole) and stirred for 2 h before cell lysis was carried out using a microfluidizer. Subsequently, this mixture was centrifuged at 100,000*g*. The resulting pellet was discarded and the supernatant was loaded onto a previously equilibrated Ni^{2+}-nitrilotriacetic agarose column (Cytvia), washed with buffer A, and eluted over 2 column volumes of buffer B (50 mM K_2HPO_4 pH 7.5, containing 100 mM NaCl and 200 mM imidazole). Fractions with the highest Rz absorbance ratio (A_{418}/A_{280}) were pooled and dialyzed overnight against buffer C (25 mM Tris pH 7.5). The next day, the protein was loaded onto a previously equilibrated weak anion exchange column (DEAE; Cytvia) and eluted over 7 CV to buffer D (25 mM Tris–HCl pH 7.5, containing 500 mM NaCl). Fractions with an Rz ratio higher than 1 were pooled, concentrated, and further purified on a S200 Sephacryl column (Cytvia) in 25 mM Tris pH 7.5. The final purified AmphL yield was >50 mg of protein per liter of *E. coli* culture with a calculated Rz of 1.3.

AmphL spectroscopic characterization

UV-visible spectra were recorded at ambient temperature on a Cary 3 spectrophotometer. P450 AmphL concentrations were determined from the Soret band absorbance in the absolute spectrum, using an absolute molar extinction coefficient (ε_{418}) of 118 mM^{-1} cm^{-1} for the low-spin oxidized form of the protein or a difference molar extinction coefficient ($\Delta\varepsilon_{448-490}$) of 91 mM^{-1} cm^{-1} for the reduced carbon monoxide complex in the difference spectra.

Crystallization of AmphL

To prepare samples for crystallography, the protein was thawed in ice and treated with 7 M equivalents of amphotericin B dissolved in DMSO (10 mM stock). The samples were subsequently buffer-exchanged into 25 mM Tris pH 7.4 using a PD-10 desalting column. The sample was concentrated to ∼30 mg/ml (∼650 μM). To assess initial crystallization conditions, crystal screenings were done using the MCSG-2 kit from Anatrace at room temperature using a Mosquito crystallization robot. The best crystallization condition was further optimized using the hanging-drop vapor diffusion method under the following conditions: a 1:1 mix of sample *versus* reservoir solution (100 mM Bis-Tris pH 7; 200 mM lithium sulfate and 25% PEG 3350) and a protein concentration of 30 mg/ml. Approximately, 1 month was required to obtain plate-like crystals. Single crystals were soaked in paratone oil and subsequently flash-frozen in liquid nitrogen. All data sets were collected at the Stanford Synchrotron Radiation Lightsource facility. The data were indexed, integrated, and scaled using XDS (15). The size of the unit cell indicated a dimer per asymmetric unit in space group $P2_12_12_1$, so the initial search was made assuming a dimer and using PimD (2XBK) as the search model and PHASER (16, 17) for molecular replacement. Refinement to 2.0 Å was carried out with Phenix.refine in the Phenix graphical interface (18, 19). Data collection and refinement statistics are shown on Table 1.

Computational methods

Molecular dynamics simulations were carried out with the GPU-optimized *pmemd.cuda* (20) in Amber 20. Substrate parameters were assigned using the GAFF force field (21) and AM1-BCC charge scheme (21, 22) as implemented in the *antechamber* module in Amber. Heme parameters were taken from Shahrokh *et al.* (23). Starting structures for MD simulations were the refined 2.0 Å structure of AmphL determined in this study and the 1.95 Å PimD-substrate complex structure 2XBK (6). The crystal structure including water molecules were immersed in an octahedral box of water with a 10 Å cushion and neutralized with Na^+ ions. The structures were conjugate gradient minimized for 1000 cycles allowing only H atoms and solvent molecules to move followed by 10,000 cycles with no restraints. Solvent was allowed to relax using constant volume heating from 5 to 300 K over 20 ps followed by a 10 ns NPT run where Cα carbon atoms were restrained by 10 kcal/mol/$Å^2$. Production runs were 100 ns with no restraints and snapshots saved every 20 ps for a total of 5000 snapshots. This was repeated 5 times for each structure using the same starting equilibrated structure but with different initial starting velocities.

Steered molecular dynamics was used to compare the unbinding reaction between AmphL and PimD. In SMD, the substrate is "pulled" or "pushed" out of the active site, and the work required as a function of distance is computed. The

Jarzynski equality (13) enables the extraction of free energy or potential of mean force from a nonequilibrium process such as the work required to push a substrate out of the active site. The vector defining the direction of push was between Cα of Ala278 in AmphL and the corresponding residue in PimD, Arg279, and one of the substrate atoms at the entry of the binding pocket. Several Cα atoms surrounding Ala278 in AmphL or Arg279 in PimD were restrained during the SMD run. This pushing vector runs approximately through the middle of the open access channel that runs parallel to the heme and the I helix. The two main variables are the rate of movement and the force of the pull. A velocity of 10 Å/ns (24) was chosen and several pulling forces ranging from 10 to 70 kcal mol^{-1} $Å^{-2}$ were tested (25) and, as others have found, the total energy required to push the substrate out of the active site was relatively insensitive to the choice of the pushing force (26). The minimum force that gave a smooth linear movement was 30 kcal mol^{-1} $Å^{-2}$. The system was prepared as in a normal MD run except after heating and equilibration, a 20 ns NVT production run was carried out where the protein and substrate atoms that defined the tail and head of the pushing vector were restrained. One hundred snapshots over that last 10 ns of the production run were used for 2.8 ns SMD runs with a pulling velocity of 10 Å/ns resulting in 28 Å push of the substrate out of the active site, and the Jarzynski average was calculated over the 100 SMD runs. Exactly the same protocol was used for PimD.

Data availability

Structure factors and coordinates have been deposited with the Protein Data Base under accession code 7SHI.

Supporting information—This article contains supporting information.

Acknowledgments—We wish to thank the Stanford Synchrotron Radiation Lab beamline staff for their support during remote data collection and Dr Huiying Li for helpful discussions on data processing. Use of the Stanford Synchrotron Radiation Lightsource, SLAC National Accelerator Laboratory, is supported by the U.S. Department of Energy, Office of Science, Office of Basic Energy Sciences under Contract No. DE-AC02-76SF00515. The SSRL Structural Molecular Biology Program is supported by the DOE Office of Biological and Environmental Research and by the National Institutes of Health, National Institute of General Medical Sciences (P30GM133894). The contents of this publication are solely the responsibility of the authors and do not necessarily represent the official views of NIGMS or NIH.

Author contributions—D. C. L. conceptualization; J. A. A., D. C. L., P. C., V. C. M., and T. L. P. investigation; S. L. K. formal analysis; S. L. K. funding acquisition; S. L. K. and T. L. P. supervision.

Funding and additional information—Work at UCI was supported by NIH grant GM131920 (T. L. P.). Funding at Swansea University was supported by the European Regional Development Fund/Welsh European Funding Office *via* the BEACON project (S. L. K.). The content is solely the responsibility of the authors and does not necessarily represent the official views of the National Institutes of Health.

Conflict of interest—The authors declare that they have no conflicts of interest with the contents of this article.

Abbreviation—The abbreviations used are: SMD, steered molecular dynamics.

References

1. Abu-Salah, K. M. (1996) Amphotericin B: An update. *Br. J. Biomed. Sci.* **53**, 122–133
2. Byrne, B., Carmody, M., Gibson, E., Rawlings, B., and Caffrey, P. (2003) Biosynthesis of deoxyamphotericins and deoxyamphoteronolides by engineered strains of Streptomyces nodosus. *Chem. Biol.* **10**, 1215–1224
3. Caffrey, P., De Poire, E., Sheehan, J., and Sweeney, P. (2016) Polyene macrolide biosynthesis in streptomycetes and related bacteria: Recent advances from genome sequencing and experimental studies. *Appl. Microbiol. Biotechnol.* **100**, 3893–3908
4. Tripathi, S., Li, H., and Poulos, T. L. (2013) Structural basis for effector control and redox partner recognition in cytochrome P450. *Science* **340**, 1227–1230
5. Lee, Y. T., Wilson, R. F., Rupniewski, I., and Goodin, D. B. (2010) P450cam visits an open conformation in the absence of substrate. *Biochemistry* **49**, 3412–3419
6. Kells, P. M., Ouellet, H., Santos-Aberturas, J., Aparicio, J. F., and Podust, L. M. (2010) Structure of cytochrome P450 PimD suggests epoxidation of the polyene macrolide pimaricin occurs *via* a hydroperoxoferric intermediate. *Chem. Biol.* **17**, 841–851
7. Poulos, T. L. (2014) Heme enzyme structure and function. *Chem. Rev.* **114**, 3919–3962
8. Gerber, N. C., and Sligar, S. G. (1994) A role for Asp-251 in cytochrome P-450cam oxygen activation. *J. Biol. Chem.* **269**, 4260–4266
9. Nagano, S., and Poulos, T. L. (2005) Crystallographic study on the dioxygen complex of wild-type and mutant cytochrome P450cam. Implications for the dioxygen activation mechanism. *J. Biol. Chem.* **280**, 31659–31663
10. Cupp-Vickery, J. R., Han, O., Hutchinson, C. R., and Poulos, T. L. (1996) Substrate-assisted catalysis in cytochrome P450eryF. *Nat. Struct. Biol.* **3**, 632–637
11. Santos-Aberturas, J., Engel, J., Dickerhoff, J., Dörr, M., Rudroff, F., Weisz, K., and Bornscheuer, U. T. (2015) Exploration of the substrate promiscuity of biosynthetic tailoring enzymes as a new source of structural diversity for polyene macrolide antifungals. *ChemCatChem* **7**, 490–500
12. Ludemann, S. K., Lounnas, V., and Wade, R. C. (2000) How do substrates enter and products exit the buried active site of cytochrome P450cam? 2. Steered molecular dynamics and adiabatic mapping of substrate pathways. *J. Mol. Biol.* **303**, 813–830
13. Jarzynski, C. (1997) Nonequilibrium equality for free energy differences. *Phys. Rev. Lett.* **78**, 2690–2693
14. Volokhan, O., Sletta, H., Ellingsen, T. E., and Zotchev, S. B. (2006) Characterization of the P450 monooxygenase NysL, responsible for C-10 hydroxylation during biosynthesis of the polyene macrolide antibiotic nystatin in Streptomyces noursei. *Appl. Environ. Microbiol.* **72**, 2514–2519
15. Kabsch, W. (2010) XDS. *Acta Crystallogr. D Biol. Crystallogr.* **66**, 125–132
16. McCoy, A. J. (2007) Solving structures of protein complexes by molecular replacement with Phaser. *Acta Crystallogr. D Biol. Crystallogr.* **63**, 32–41
17. McCoy, A. J., Grosse-Kunstleve, R. W., Adams, P. D., Winn, M. D., Storoni, L. C., and Read, R. J. (2007) Phaser crystallographic software. *J. Appl. Crystallogr.* **40**, 658–674
18. Adams, P. D., Afonine, P. V., Bunkoczi, G., Chen, V. B., Echols, N., Headd, J. J., Hung, L. W., Jain, S., Kapral, G. J., Grosse Kunstleve, R. W., McCoy, A. J., Moriarty, N. W., Oeffner, R. D., Read, R. J., Richardson, D. C., *et al.* (2011) The Phenix software for automated determination of macromolecular structures. *Methods* **55**, 94–106
19. Echols, N., Grosse-Kunstleve, R. W., Afonine, P. V., Bunkoczi, G., Chen, V. B., Headd, J. J., McCoy, A. J., Moriarty, N. W., Read, R. J., Richardson,

D. C., Richardson, J. S., Terwilliger, T. C., and Adams, P. D. (2012) Graphical tools for macromolecular crystallography in PHENIX. *J. Appl. Crystallogr.* **45**, 581–586
20. Mermelstein, D. J., Lin, C., Nelson, G., Kretsch, R., McCammon, J. A., and Walker, R. C. (2018) Fast and flexible gpu accelerated binding free energy calculations within the amber molecular dynamics package. *J. Comput. Chem.* **39**, 1354–1358
21. Wang, J., Wolf, R. M., Caldwell, J. W., Kollman, P. A., and Case, D. A. (2004) Development and testing of a general amber force field. *J. Comput. Chem.* **25**, 1157–1174
22. Jakalian, A., Jack, D. B., and Bayly, C. I. (2002) Fast, efficient generation of high-quality atomic charges. AM1-BCC model: II. Parameterization and validation. *J. Comput. Chem.* **23**, 1623–1641
23. Shahrokh, K., Orendt, A., Yost, G. S., and Cheatham, T. E., 3rd (2012) Quantum mechanically derived AMBER-compatible heme parameters for various states of the cytochrome P450 catalytic cycle. *J. Comput. Chem.* **33**, 119–133
24. Park, S., and Schulten, K. (2004) Calculating potentials of mean force from steered molecular dynamics simulations. *J. Chem. Phys.* **120**, 5946–5961
25. Ho, K., Truong, D. T., and Li, M. S. (2020) How good is Jarzynski's equality for computer-aided drug design? *J. Phys. Chem. B* **124**, 5338–5349
26. Zhang, Z., Santos, A. P., Zhou, Q., Liang, L., Wang, Q., Wu, T., and Franzen, S. (2016) Steered molecular dynamics study of inhibitor binding in the internal binding site in dehaloperoxidase-hemoglobin. *Biophys. Chem.* **211**, 28–38